Sensors and Actuators B 255 (2018) 1031–1038

Contents lists available at ScienceDirect

Sensors and Actuators B: Chemical

journal homepage: www.elsevier.com/locate/snb

Research Paper

Printed-Sensor-on-Chip devices – Aerosol jet deposition of thin film relative humidity sensors onto packaged integrated circuits

Ben Clifford, David Beynon*, Christopher Phillips, Davide Deganello

Welsh Centre for Printing and Coating, College of Engineering, Swansea University, Swansea, SA1 8EN, UK

ARTICLE INFO

Article history:
Received 28 March 2017
Received in revised form 13 July 2017
Accepted 9 August 2017
Available online 24 August 2017

Keywords:
Sensor-on-Chip
Aerosol jet deposition
Printed electronics
Humidity sensor
Nafion

ABSTRACT

In this paper we report on the development of an aerosol jet printed sensing platform integrating elements of silicon and printed electronics. To demonstrate the technology, thin film humidity sensors have been fabricated over the top surface and sides of pre-packaged integrated circuits using a combination of direct-write aerosol jet deposition and drop-casting. The resistive based sensor consists of an aerosol jet deposited interdigitated nano-particle silver electrode structure overlaid with a thin film of Nafion® acting as a humidity sensitive layer. The fabricated sensor displayed a strong response to changes in relative humidity over the tested range (40% RH–80% RH) and showed a low level of hysteresis whilst undergoing cyclic testing. The successful fabrication of relative humidity sensors over the surface and pins of a packaged integrated circuit demonstrates a new level of integration between printed and silicon based electronics – leading to Printed-Sensor-on-Chip devices. Whilst demonstrated for humidity, the proposed concept is envisaged to work as a platform for a wide range of applications, from bio-sensing to temperature or gas monitoring.

1. Introduction

In this paper, we present the use of aerosol jet deposition (AJD) to create microscale printed sensors directly onto pre-packaged integrated circuits (IC's). The approach used demonstrates a new way of integrating elements of printed and silicon electronics adding additional functionality to the silicon device, and resulting in complete miniaturised sensor systems. This novel sensor fabrication process is demonstrated by printing a relative humidity sensor over the top surface and edges of an analogue-to-digital converter (ADC) integrated circuit, demonstrating the concept of Printed-Sensor-on-Chip devices.

The prospect of mass produced completely printed electronic systems is attractive, however it is still in the early stages of development [1,2]. Whilst the use of printing and other related deposition technologies to produce sensors is currently achievable [3–6], in order to be of use, these sensors still require the use of conventional silicon electronics control elements [7,8]. A key challenge to working with printed electronics and sensors is how these printed and silicon elements are integrated together and the limitations arising from this. Due to temperature constraints and mechanical reasons, common silicon integration methods, such as solder bonding, wire bonding and flip-chip assembly, are not suitable for use with flexible printed electronics [9,10].

In this paper a different approach is demonstrated based on fabrication by AJD of small scale sensors over silicon components – a solution capable of joining the functionality and advanced materials of printed electronics with the maturity and processability of conventional silicon based electronics. By integrating customisable printed sensors directly onto integrated circuits new application specific integrated circuits (ASIC's) can be developed and still processed using conventional electronics assembly techniques. Additionally, the overall footprint and weight of the device are reduced when compared with a separate sensor system attached/integrated via a cable to a silicon control circuit. The approach of using additive deposition methods (with a variety of processes cited) has been previously outlined in a patent application by Texas Instruments but has not been physically demonstrated [11].

AJD is a direct-write additive fabrication technology capable of depositing a wide range of functional materials without the need for conventional masks and/or stencils [12]. The aerosol jet process works by atomising a solution/suspension containing a functional material into a fine mist of droplets which are suspended in a carrier gas flow. The generated mist is then transported to a deposition head where it is focused into a collimated stream by a secondary

* Corresponding author.
E-mail address: d.g.beynon@swansea.ac.uk (D. Beynon).

http://dx.doi.org/10.1016/j.snb.2017.08.086

gas flow and directed towards the substrate through a converging nozzle. The substrate is positioned below the nozzle on a motion controlled heated stage and patterning is achieved by the relative movement of the substrate and deposition head [13–16]. The process is non-contact, enabling features to be printed onto both two- and three-dimensional surfaces. AJD is therefore capable of patterning functional materials over challenging topographies, such as the surface and edges of an IC, which would not be possible with other printing processes. These capabilities allow the technology to be used in the fabrication of a wide range of highly customisable printed electronic devices and sensors. The technology has been reported in journal articles as a deposition method for functional layers in a diverse range of applications including thin film transistors [17–19], strain gauges [20], solar cells [21–25], light emitting diodes (LED's) [22,26], printed circuits [27], resonators [28] and biological sensors [6].

On account of its non-contact, digital nature and ability to deposit over non-conformal surfaces, AJD is an ideal process for the development of the proposed Printed-Sensor-on-Chip technology. However, despite the advantages offered by AJD, there were a number of challenges in terms of overcoming the non-conformal and complex topography of the pre-packaged IC. These included careful control of a number of process parameters to maintain track consistency over the relatively rough surfaces and steep walls.

To provide a demonstration of the capabilities of this technology, a relative humidity sensor was fabricated over a pre-packaged analogue-to-digital converter. AJD was adopted for depositing the microscale interdigitated electrodes and interconnects. Nafion® was used as the functional humidity sensitive material, drop cast over the AJD interdigitated electrodes. As the relative humidity of the environment increases, the level of water adsorbed into the Nafion® film rises. This causes dissociation of the acidic sites and through the presence of water molecules, proton hopping occurs decreasing the resistance of the layer. As the relative humidity decreases, the opposite effect is observed with little dissociation of the acidic groups taking place, resulting in a lower number of conductive pathways [29–31].

2. Experimental

2.1. Materials

The interdigitated electrode structure was deposited using a commercial nano-particle silver ink TPS 35 HE (Clariant Produkte (Deutschland) GmbH). This ink was diluted with deionised water at a ratio of 1:3 parts by volume and stored at 4 °C when not in use. The active layer was produced using a 20 wt.% Nafion® solution in a mixture of lower aliphatic alcohols and water (Sigma-Aldrich 527122). This material was used without further modification to produce thin films. Prior to the deposition of the interdigitated electrodes, the surface of the IC package was cleaned with ≥99.8% absolute Ethanol (Sigma-Aldrich, 24103) to remove any contaminants/trace materials from the manufacturing process.

The integrated circuit used was an MCP3001 10-bit analogue-to-digital converter (Microchip Technology Inc., USA) in a standard narrow SOIC-8 footprint. The top surface of the chip body has an area of 4.90 mm by 3.90 mm with chamfered edges on all sides [32]. The electrode digits/fingers are deposited on the horizontal surface of the chip body whilst the connections to the chip pins are printed via the chip shoulder and edge at ≈45° and ≈80° respectively – relative to the top surface. The surface of the chip is made from a rough moulded resin and is engraved with text indicating the model number of the chip and an identifier for pin 1. The average surface roughness (Sa) and the maximum surface height (Sz) were measured at 1.09 μm and 8.80 μm respectively in accordance with EN ISO 4287 using an Alicona G5 Infinite Focus optical microscope (Alicona Imaging GmbH). The average depth of the engraved text was measured to be of the order of 13 μm, which provided a step over which print continuity had to be maintained. In addition to being a low cost and mass produced integrated circuit, the MCP3001 was chosen for its ability to perform conversions based on a low reference voltage (0.25 V – Vdd). Operation of the sensor at low voltages is essential to avoid unwanted decomposition of the water by the applied voltage – water is decomposed when the applied potential difference is greater than ≈1.2 V [33].

2.2. Sensor design and fabrication

The Printed-Sensor-on-Chip platform consists of an interdigitated electrode structure which was overlaid with an active sensing material specific to the intended application. The interdigitated electrode structure was deposited by aerosol jet deposition on the top surface of the integrated circuit and included interconnects which extend over the edge of the package and onto the required pins of the IC. For the application presented, the printed sensor makes contact with pins two and four of the IC. The individual electrodes are designed to be 2.2 mm in length and have a width and separation of 100 μm. The interdigitated design was chosen to provide the largest effective active area for the sensor and for this application measures 2.7 mm by 2.3 mm. The interdigitated electrode structure comprises of multiple interdigitated electrodes and two interconnects. Each interconnect provides a channel that connects the interdigitated electrodes to the required pins of the IC. Given the function of these interconnects they were designed with a width of 150 μm to maintain a high conductivity over the edge of the chip package.

The interdigitated electrode structure was produced using an AJ300 aerosol jet deposition system (Optomec Inc., USA) an overview of which is shown in Fig. 1. During deposition a ceramic nozzle with a 100 μm diameter orifice was used. Deposition was carried out using an ultrasonic atomiser operating at a frequency of 2.4 MHz and was driven at 48 V and 660 mA to generate a dense mist of droplets. This mist was transported via a gas stream (atomiser flow) through a length of tubing to the deposition head at which point the entrained droplet stream was surrounded by a secondary gas flow known as the sheath gas and directed towards the substrate through the nozzle. The platform movement was then moved at controlled speeds to pattern the silver ink on both top surface and chip edges.

Following deposition of the interdigitated electrode structure, the "printed-on" integrated circuit was placed in a convection oven to drive off any remaining solvent and to sinter the nano-particle deposit and hence impart conductivity to the electrode structure.

Printing of the interdigitated structure and connects to the chip pins presented challenges in terms of maintaining conductivity when printing over the rough surface and steep walls of the IC, presenting a range of working distances between the nozzle and the IC, a parameter known to affect print quality, as well as producing sufficient definition in the electrode digits so that both width and gaps were controlled. There are also a host of process parameters that affect deposition generally that must be optimized for each ink system used. A series of deposition tests were therefore carried out using glass microscope slides as a standard substrate to understand the effects of various process parameters and to identify the optimal values for printing high resolution features on the IC package.

Scanning Electron Microscopy (SEM) analysis was performed using a JEOL 7800 Field Emission Gun Scanning Electron Microscope to look at the morphology of the sintered nano-particle silver layer. Additionally, the resistance of the sintered silver layer was measured using a probe station with micro-positioners connected

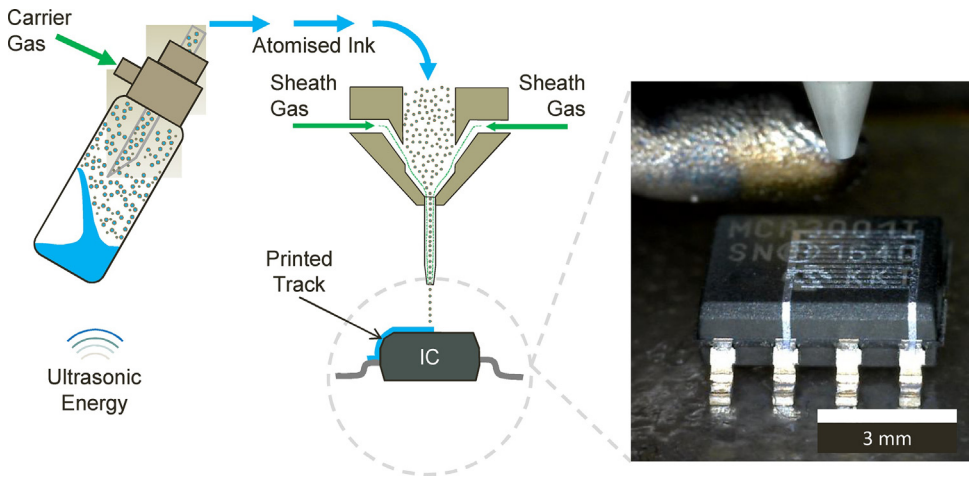

Fig. 1. Schematic of the Aerosol Jet Deposition Process Showing the Fabrication of an Interdigitated Electrode Structure over an Integrated Circuit.

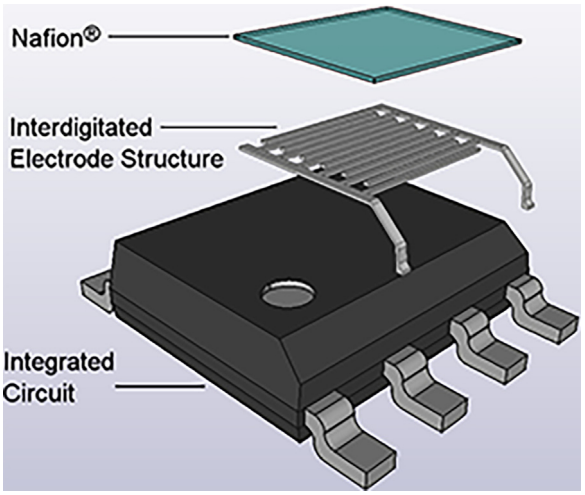

Fig. 2. An exploded 3D representation of the sensor showing the Aerosol Jet Deposited Interdigitated Electrode Structure and Nafion® Layer.

to a Keithley 2000 multimeter. The first probe was positioned on the pin of the IC and the second at the furthest point along the top most interdigitated electrode. This measurement was performed on both sides of the interdigitated electrode structure from pins two and four.

To complete the sensor, using a mechanical pipette, a layer of Nafion® was drop cast over the interdigitated electrodes creating an electrical connection. Drop casting was selected as a rapid means of depositing a coating as selective patterning was not required. A casting volume of 0.5 μl was used and was deposited at a distance of 1 mm above the chip surface. The cast films were allowed to dry at room temperature for at least 12 h prior to characterisation of the sensor. The resistance of the fabricated sensor was then proportional to the relative humidity of the environment. Fig. 2 shows an exploded 3D representation of the sensor showing the AJD Interdigitated Electrodes and Nafion® layer relative to the IC.

2.3. Sensor operation and measurement

The Vss and Vref pins of the IC were connected to a dual channel power supply (Rohde & Schwarz GmbH & Co KG (Germany)) which provided five volts and one volt to the pins respectively. With Vref, set to one volt and using the full 10-bit resolution of the ADC the sensor is capable of measuring changes in voltage as low as 0.97 mV. Using a serial interface the sensor can be enabled or disabled and measured using a microcontroller (MCU) and data acquisition system (DAQ). To enable the sensor, the MCU sends a low signal to the ADC's chip select (~CS) pin, two pulses of the clock signal then initiate a measurement by the ADC. The MCU then successively reads 10 bits of data from Dout, one bit per clock pulse, before setting the chip select pin high – disabling the sensor. The serial data is reassembled by the MCU and transmitted to a PC where it is recorded against the current timestamp and plotted in real-time. A circuit schematic for the MCP3001 ADC is shown in Fig. 3, showing (a) the use of a traditional potential divider and (b) the position and connections of the printed sensor when integrated with the ADC. The sensitivity of the sensor system was tuned by varying the value of R1 against the variable resistance R2 and for the presented application R1 was selected to be 10 MΩ. When the variation in R2 is large and spans multiple orders of magnitude (ohms–mega ohms) the value chosen for R1 significantly influence the sensitivity at one end of the measurement scale when compared to the other.

The sensor was installed into the circuit described above and placed into a Sanyo MTH-2400 environmental chamber at a constant temperature of 20 °C. To verify the humidity and temperature at the position of the sensor within the chamber, an additional humidity logger (LASCAR electronics EL-USB-2-LCD+) was used to simultaneously record temperature and humidity data in parallel with the Printed-Sensor-on-Chip. This logger was rated for operation between −35 °C and 80 °C at 0% RH–100% RH with an accuracy of ±0.3 °C and ±2% RH [34]. The sensor was subjected to testing, cycling the relative humidity between 40% RH and 80% RH. This allowed the hysteresis and repeatability characteristics of the sensor to be determined. In addition, incremental tests were performed to evaluate the step response of the printed sensor at intervals of 10% RH. Data values were recorded every ten seconds synchronised with the capabilities of the LASCAR reference logger. The experimental setup is shown in Fig. 4.

3. Results and discussion

3.1. Optimization of print parameters

The amount of ink deposited as well as the quality of deposition, were controlled by adjusting key process parameters including; the flow rate of the atomiser and sheath gas streams, the speed of stage

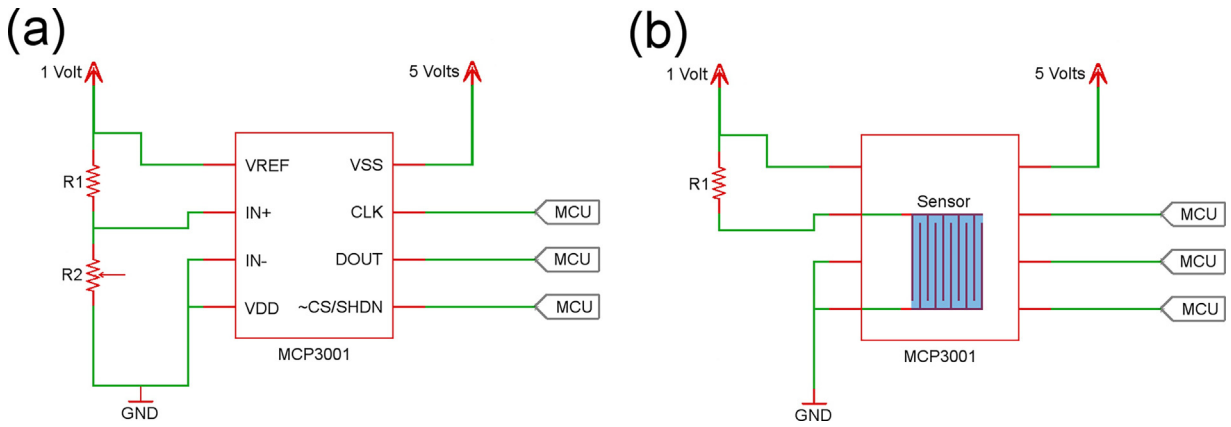

Fig. 3. MCP3001 Circuit Schematic (a) With a Variable Resistor and (b) With the Printed Sensor.

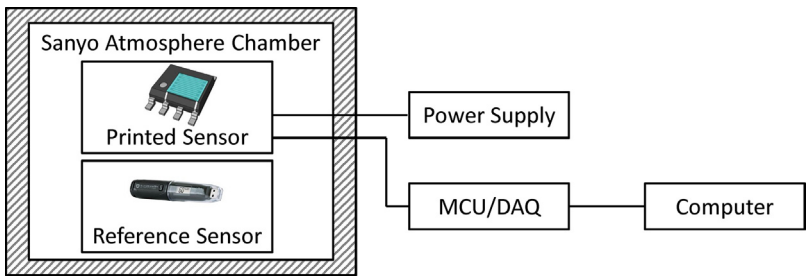

Fig. 4. Experimental Setup used to Measure the Response of the Printed-Sensor-on-Chip Device to Changes in Humidity.

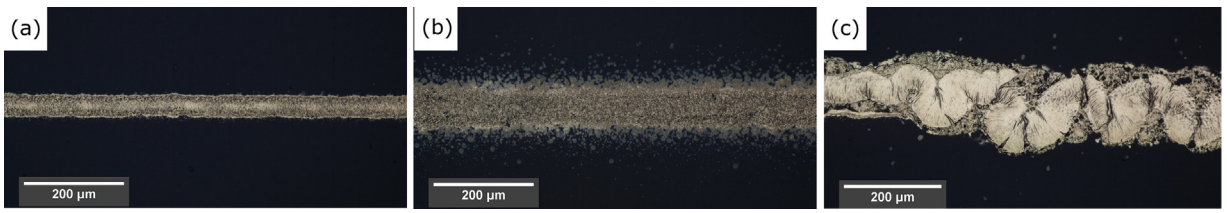

Fig. 5. The effect of varying process parameters on deposition quality – (a) Optimised Focusing Ratio, (b) Poor quality line due to turbulent flow within the nozzle and (c) Excessive deposition from a too high atomiser flow.

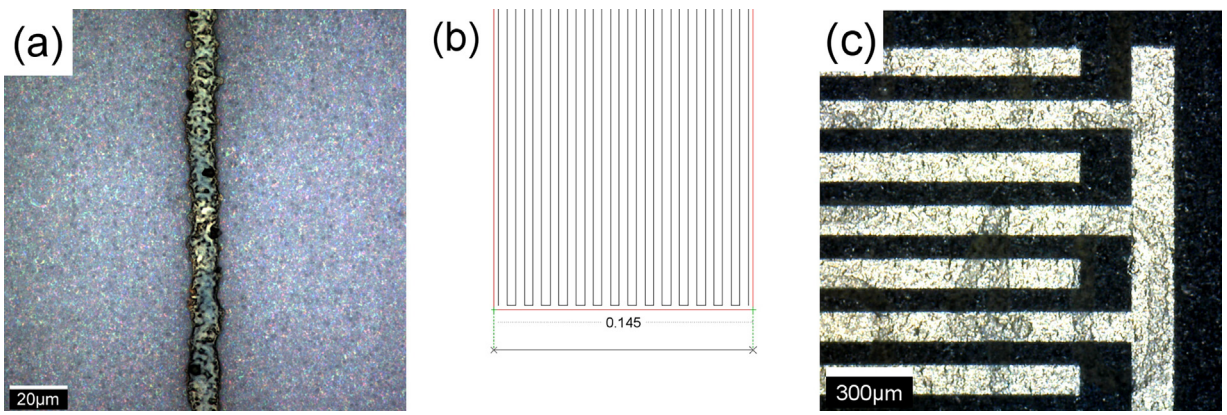

Fig. 6. Optimisation of Aerosol Jet Parameters (a) Showing a 10 µm Wide Line Deposited at 2 mm/s on a Glass Substrate (scale bar is 20 µm), (b) The Parallel Line Fill Pattern used to Produce Wider Lines, and (c) The Interdigitated Electrode Structure Deposited on the Chip Surface (scale bar is 300 µm).

movement and the number of passes used. Since adjustments in gas flows require a stabilization period before laminar flow is reached, these had to be fixed prior to printing. The atomiser flow rate acted as the main determinant of the amount of material flow from the nozzle while the sheath flow acted to focus the material stream into a collimated beam. If the atomiser flow rate is too low, insufficient material is deposited, on the other hand a high atomiser flow rate results in excessive and erratic material deposition as shown in Fig. 5(c). As the focussing ratio (sheath gas flow rate/atomiser gas flow rate) was increased to an optimal level, the line width was

reduced and the definition of printed edges improved. However, further increases in focussing ratio, passed the optimum, lead to the introduction of "overspray" – a phenomenon whereby material is deposited outside the target area due to turbulent flow causing wider unfocussed lines Fig. 5(b). Optimal values for the atomiser and sheath gas flow rates were found to be 14 cm^3/min and 32 cm^3/min respectively. These settings allowed the deposition of high resolution fine lines with minimal "overspray". This is illustrated in Fig. 6(a) which shows printed lines of silver ink with an average width of 9.8 μm.

Given the need to produce conductive features over the non-conformal topography of the IC package, the stage speed was investigated as a means of controlling the amount of ink deposited on the various sections of the IC package. Using the optimal flow rates described above, as the stage speed was increased from 1 to 3 mm/s, the width of the deposited line decreased slightly but at greater speeds (3–10 mm/s), the line width was found to be independent of stage speed. In terms of the thickness of ink deposit, there was a decrease as stage speed was increased with an especially rapid drop in thickness between speeds of 1 and 3 mm/s. This indicated that stage speed could be adjusted to compensate for the lower material deposition that occurs when the nozzle and IC surface are not perpendicular as when printing down the side of the IC and onto the pins. Platform movement speeds of 2.5 mm/s and 0.8 mm/s were therefore used for the top surface and chip edges respectively. To overcome the surface roughness of the IC package and to ensure good coverage and low resistance over the entire print, the print cycle was repeated five times giving an approximate print thickness of 1.8 μm.

Variation of the working distance, the nozzle to substrate gap, between 2 and 5 mm was seen to have little effect in the width of deposited lines. However, as the working distance was increased further, the width of the deposited line tended to increase. In terms of thickness of the ink deposit, there was again very little variation in the 2–5 mm range but as distance was increased this thickness fell. More significantly, larger working distances gave poorly defined edges and demonstrable overspray. Given the size of the IC used in this experiment, it was possible to maintain the working distance to the IC package between two and four millimetres over the pins and top surface without adjustment of the nozzle height.

Without the use of stage heating, there was a tendency for migration of material to the edges of the line during drying (coffee-stain effect). The use of stage heating reduced this effect allowing almost rectangular line profiles at 100 °C.

Rather than directly printing 100 micron wide lines for the interdigitated electrode structure, multiple fine lines were printed parallel to each other in a serpentine fashion with a narrow separation as shown in Fig. 6(b). This produced features with high edge definition and low amounts of overspray. Fig. 6(c) shows the deposited 100 μm and 150 μm wide lines printed on the chip surface.

Heating of the deposited silver tracks causes the nano-particles to sinter together forming a conductive layer with a low resistance. Maximum print conductivity was obtained by heating the deposited layers at 200 °C for 60 min in a convection oven.

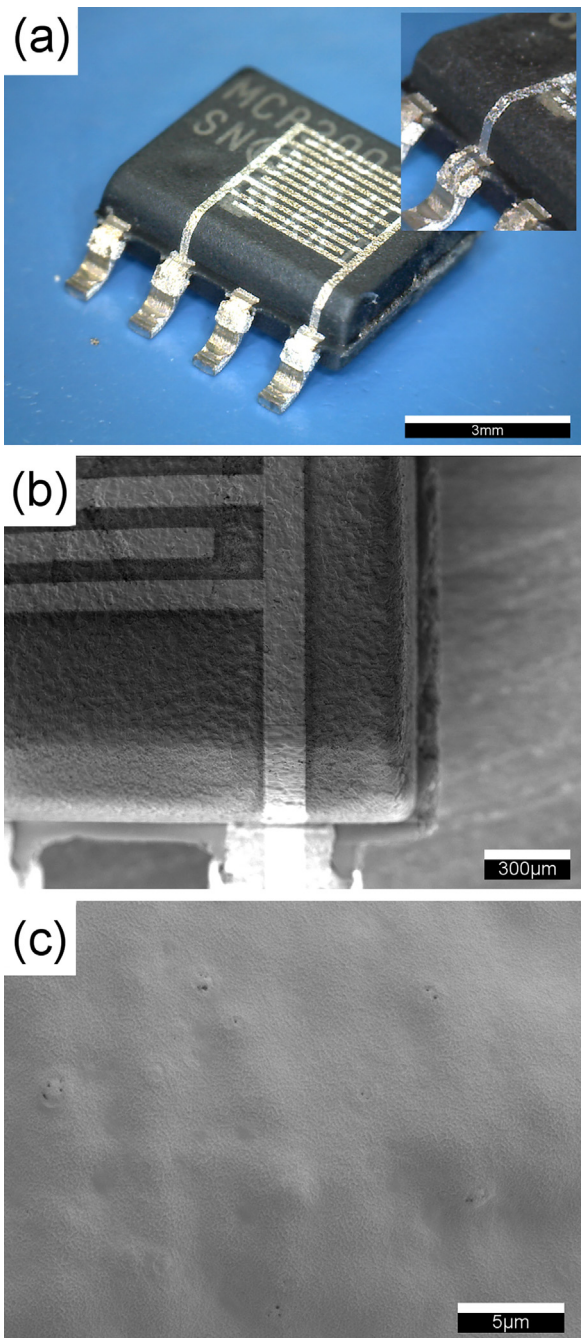

Fig. 7. (a) A Photograph Showing the Aerosol Jet Deposited Interdigitated Electrode Structure Over the Chip Surface with an Inset Focusing on the Chip Edge Region, (b, c) SEM Images of the Deposited Interdigitated Electrode Structure over the Chip Surface and Edges at 60× and 3000× magnification respectively.

3.2. Characterization of the interdigitated electrode structure

The print settings used produced well defined features that coped with the topography of the chip. The resistance from pin 2 to the furthest point on the top most electrode measured 16.1 Ω and from pin 4 to the furthest point on the top most electrode measured 18.5 Ω. Fig. 7(a) is a photograph of the deposited interdigitated electrode structure showing the interconnects extending over the edge of the IC package and making contact with the chip pins. The inset image shows an enlarged photograph of the chip edge, showing the continuity of the aerosol jet deposited silver layer over the steep angle. Fig. 7(b) and (c) are SEM images of the sintered nano-particle silver taken at 60× and 3000× magnification respectively. Fig. 7(b) provides an overview of the interdigitated electrode structure focusing on the edge of the chip revealing no change in morphology when printing over the edge. Fig. 7(c) shows the morphology of the silver layer displaying a film like structure representative of a completely sintered layer. The high quality of the sintered layer can be seen with no pin-holes or micro-cracks being observed.

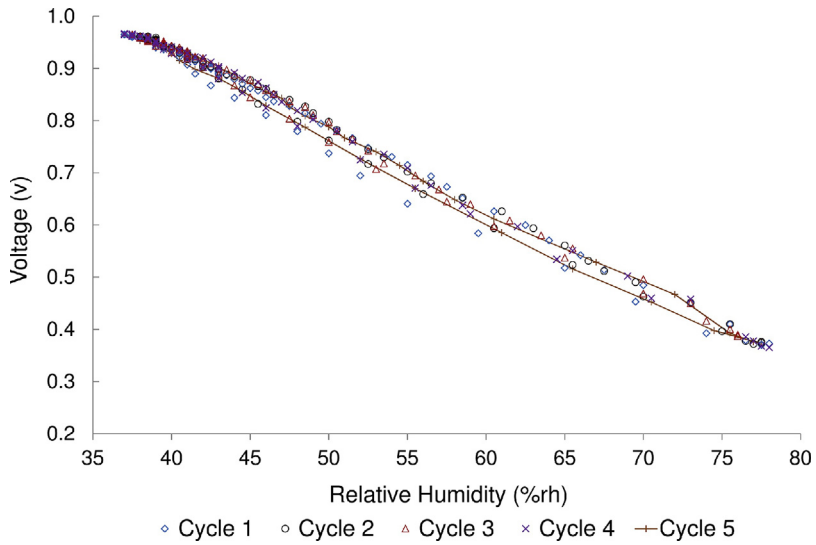

Fig. 8. The Hysteresis of the Printed-Sensor-on-Chip Device Measured from 40% RH to 80% RH and Back to 40% RH for five cycles. Vss = 5 V, Vref = 1 V and R1 = 10 MΩ.

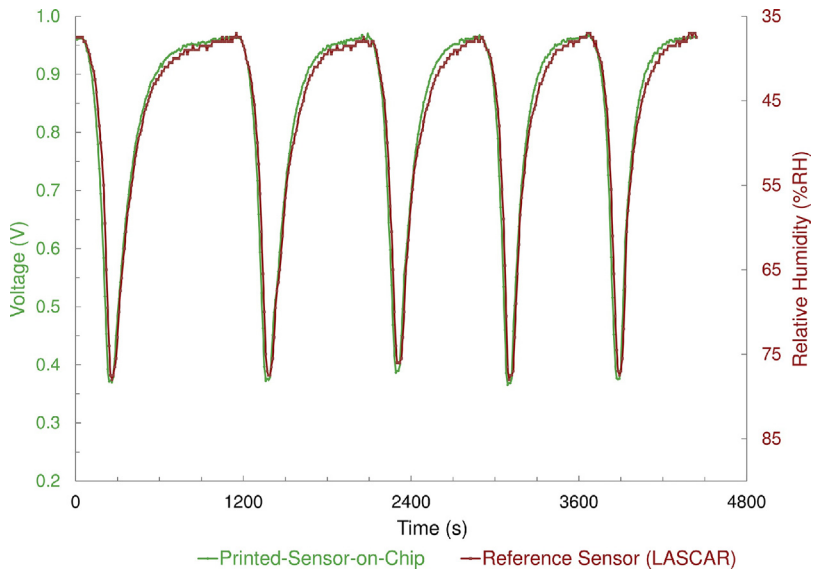

Fig. 9. The Repeatability Characteristic of the Printed-Sensor-on-Chip Device Measured from 40% RH to 80% RH and Back to 40% RH for five cycles. Vss = 5 V, Vref = 1 V and R1 = 10 MΩ.

3.3. Humidity response of the Printed-Sensor-on-Chip device

The humidity of the chamber was cycled between 40% RH and 80% RH and data was recorded from both the Printed-Sensor-on-Chip device and the LASCAR reference sensor. After a stabilization period of 15 min at 40% RH and 20 °C in the environmental chamber, the humidity value was cycled between 40% RH and 80% RH and back down whilst a constant 20 °C temperature was maintained. Measurements of both the Printed-Sensor-on-Chip device and the reference sensor (LASCAR) were taken at 10 s intervals and the test was repeated five times. Fig. 8 shows a plot of the voltage output recorded from the Printed-Sensor-on-Chip device against the relative humidity value recorded by the reference sensor. From this, the hysteresis response of the device can be seen, exhibiting a linear trend with an R2 value of 0.9959 on cycle 5 ($y = -0.0153x + 1.5438$). Looking at the data for cycle five the maximum hysteresis is calculated to be 3.7% at 48.5% RH with no significant variation over the entire range. The first cycle shows a slightly broader hysteresis when compared with cycles 2–5 suggesting a conditioning period is beneficial following fabrication. Fig. 9 shows repeatable results from the Printed-Sensor-on-Chip device across the five cycles, as well as a close agreement with the measurements obtained from the reference senor.

Again, after a stabilization period of 15 min at 40% RH and 20 °C in the environmental chamber, the humidity value was stepped from 40% RH to 80% RH and back down in 10% RH increments. At each increment the environmental chamber was allowed to stabilize for 5 min before the relative humidity value was changed. Measurements of both the Printed-Sensor-on-Chip device and the reference sensor (LASCAR) were taken periodically at 10 s intervals and the results are shown in Fig. 10. The data shows that the response of the Printed-Sensor-on-Chip device is nonlinear with respect to changes in the relative humidity of the environment. The change in voltage (and hence resistance) are larger for changes at higher relative humidity (70% RH–80% RH) compared against lower relative humidity. This behaviour has been previ-

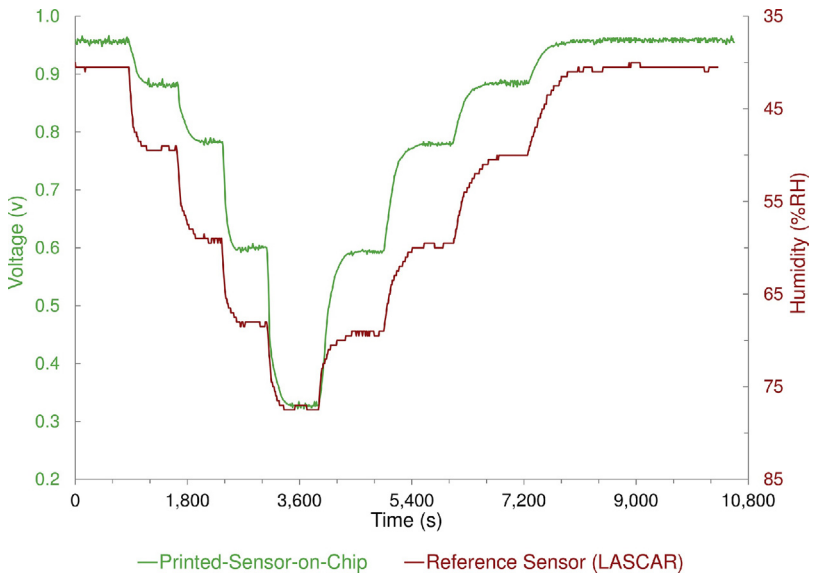

Fig. 10. The Response of the Printed-Sensor-on-Chip Device Measured from 40% RH to 80% RH and Back to 40% RH in 10% RH step increments. Vss = 5 V, Vref = 1 V and R1 = 10 MΩ.

ously observed when using Nafion® as the sensing material and the results obtained from the Printed-Sensor-on-Chip are comparable to those reported in literature [35,36].

3.4. Discussion

The presented printed-sensor-on-chip demonstrated a sensitive response to changes in humidity. The deposition of the interdigitated electrode structure overcame the difficulties in printing onto a challenging 3D structure. In order to further develop and expand the proposed concept of printed-sensor-on-chip to a larger manufacturing scale, it is essential to assess all its components.

The interdigitated electrode structure is made up of multiple overlapping parallel lines meaning the overall device/sensor size can be reduced, allowing further miniaturization. This would allow the use of chips with smaller footprints, as well as the fabrication of multiple sensing elements on a single chip. Similar interdigitated structures could be also employed for integration onto the chips not only of sensors, as here demonstrated, but also other electronic components such as interdigitated supercapacitors for energy storage [37,38]. In this case, aerosol jet printed silver could be used as a current collector which could then be overlaid with an ink containing an energy storing material, such as activated carbon.

In order to sinter the printed silver ink, the device has to withstand a heating process and the temperatures used in this work may cause failure in more sensitive chips; although this was not observed during the study. This processing temperature could be significantly reduced by using lower temperature sintering inks, as found in other printing processes; however, currently there is not a wide range of conductive inks tailored to the aerosol jet deposition process. Another approach would be to investigate the use of alternative rapid sintering technologies such as Near-Infrared (NIR) or photonic sintering [39,40].

Finally deposition of the sensing material, Nafion® could be improved by using automated drop-on-demand systems.

4. Conclusions

In this paper, for the first time, the use of aerosol jet deposition to create printed sensors directly onto pre-packaged integrated circuits has been demonstrated. This provides a way of integrating printed and silicon electronics to form individually customisable application specific integrated circuits that are compatible with traditional electronics/PCB manufacturing and assembly processes. The ability to produce a high resolution interdigitated electrode structure over a rough and non-conformal surface has been demonstrated whilst maintaining a high conductivity. Additionally, AJD was used to deposit conductive tracks directly over the edges of an integrated circuit package, overcoming the steep angle, joining the printed sensor with the IC connections.

The Printed-Sensor-on-Chip concept has been successfully demonstrated through the fabrication of a relative humidity sensor printed on the top surface of an analogue-to-digital converter IC. The relative humidity sensor displayed a strong response to changes in relative humidity tested between 40% RH and 80% RH as well as showing low hysteresis and good repeatability characteristics. However, the approach described is a platform technology that can be adapted to individual application requirements simply by adjusting the IC, design or materials.

The Printed-Sensor-on-Chip allows devices to be fabricated with smaller footprints by vertically integrating components onto traditional electronic IC's. Advances in this area will extend the technology to printing entire miniaturised circuits vertically integrated on top of conventional electronic components and PCB's. This technology inspires a vision enabling opportunities for new markets creating individually customised/fingerprinted circuits and devices that can still be commercially processed and constructed.

Acknowledgments

This project was supported by the EPSRC (UK) grant number EP/N013727/1. SEM facilities were provided by the Swansea University AIM Facility; funded in part by the EPSRC (EP/M028267/1), the European Regional Development Fund through the Welsh Government (80708) and the Ser Solar project via Welsh Government. This work was also financially supported by the College of Engineering at Swansea University. We would also like to acknowledge the Centre for Nano Health (CNH) at Swansea University for access to facilities and equipment.

References

[1] H.-E. Nilsson, T. Unander, J. Sidén, H. Andersson, A. Manuilskiy, M. Hummelgård, M. Gulliksson, System integration of electronic functions in smart packaging applications, IEEE Trans. Compon. Packag. Manuf. Technol. 2 (October (10)) (2012) 1723–1734.

[2] V. Subramanian, J.B. Chang, A. de la Fuente Vornbrock, D.C. Huang, L. Jagannathan, F. Liao, B. Mattis, S. Molesa, D.R. Redinger, D. Soltman, S.K. Volkman, Q. Zhang, Printed electronics for low-cost electronic systems: technology status and application development, in: Solid-State Circuits Conference, 2008. ESSCIRC 2008. 34th European, Edinburgh, 2008.

[3] A.K. Assaifan, J.S. Lloyd, S. Samavat, D. Deganello, R.J. Stanton, K.S. Teng, Nanotextured surface on flexographic printed ZnO thin films for low-cost non-faradaic biosensors, ACS Appl. Mater. Interfaces 8 (49) (2016) 33802–33810.

[4] Y. Mouhamad, T. Mortensen, A. Holder, A.R. Lewis, T.G. Maffeis, D. Deganello, High performance tunable piezoresistive pressure sensor based on direct contact between printed graphene nanoplatelet composite layers, RSC Adv. 6 (107) (2016).

[5] F. Molina-Lopez, D. Briand, N.F. de Rooij, All additive inkjet printed humidity sensors on plastic substrate, Sens. Actuators B 166–167 (2012) 212–222.

[6] I. Grunwald, E. Groth, I. Wirth, J. Schumacher, M. Maiwald, V. Zoellmer, M. Busse, Surface biofunctionalization and production of miniaturized sensor structures using aerosol printing technologies, Biofabrication 2 (March (1)) (2010) 014106.

[7] J. Perelaer, P.J. Smith, D. Mager, D. Soltman, S.K. Volkman, V. Subramanian, J.G. Korvink, U.S. Schubert, Printed electronics: the challenges involved in printing devices, interconnects, and contacts based on inorganic materials, J. Mater. Chem. 20 (June (39)) (2010) 8446–8453.

[8] Organic and Printed Electronics Association, Organic and Printed Electronics: Applications, Technologies and Suppliers 5th Edition, 5th ed., VDMA Verlag GmbH, sdfgfg, 2013.

[9] L. Xie, Heterogeneous Integration of Silicon and Printed Electronics for Intelligent Sensing Devices, KTH School of Information and Communication Technology, Stockholm, 2014.

[10] J.-N. Aoh, C.-L. Chuang, M.-Y. Kang, Reliability of TCT and HH/HT test performed in chips and flex substrates assembled by thermosonic flip-chip bonding process, Microelectron. Reliab. 53 (3) (2013) 463–472.

[11] B.S. Cook, J.A. Herbsommer, D. Trombley, S.A. Kummerl, A. Emerson, Semiconductor package with printed sensor. United States of America Patent US20160093548 A1, 31 03 2016.

[12] Y. Zhang, C. Liu, D. Whalley, Direct-write techniques for maskless production of microelectronics: a review of current state-of-the-art technologies, Electronic Packaging Technology & High Density Packaging, 2009. ICEPT-HDP '09. International Conference on, Beijing (2009).

[13] A. Mahajan, C.D. Frisbie, L.F. Francis, Optimization of aerosol jet printing for high-resolution, high-aspect ratio silver lines, ACS Appl. Mater. Interfaces 5 (May (11)) (2013) 4856–4864.

[14] M. Smith, Y.S. Choi, C. Boughey, S. Kar-Narayan, Controlling and assessing the quality of aerosol jet printed features for large area and flexible electronics, Flexible Printed Electron. 2 (February (1)) (2017) 27.

[15] S. Binder, M. Glatthaar, E. Rädlein, Analytical investigation of aerosol jet printing, Aerosol Sci. Technol. 48 (9) (2014) 924–929.

[16] M. Mashayekhi, L. Winchester, L. Evans, T. Pease, M.-M. Laurila, M. Mäntysalo, S. Ogier, L. Terés, J. Carrabina, Evaluation of aerosol, superfine inkjet, and photolithography printing techniques for metallization of application specific printed electronic circuits, IEEE Trans. Electron Device 63 (3) (2016) 1246–1253.

[17] C.S. Jones, X. Lu, M. Renn, M. Stroder, W.-S. Shih, Aerosol-jet-printed, high-speed, flexible thin-film transistor made using single-walled carbon nanotube solution, Microelectron. Eng. 87 (March (3)) (2010) 434–437.

[18] R. Liu, F. Shen, H. Ding, J. Lin, W. Gu, Z. Cui, T. Zhang, All-carbon-based field effect transistors fabricated by aerosol jet printing on flexible substrates, J. Micromech. Microeng. 23 (May (6)) (2013) 065027.

[19] S.H. Kim, K. Hong, K.H. Lee, C.D. Frisbie, Performance and stability of aerosol-jet-printed electrolyte-gated transistors based on poly(3-hexylthiophene), ACS Appl. Mater. Interfaces 5 (June (14)) (2013) 6580–6585.

[20] M. Maiwald, C. Werner, M. Busse, V. Zoellmer, INKtelligent printed strain gauges, Sens. Actuator A: Phys. 162 (August (2)) (2010) 198–201.

[21] P. Kopola, B. Zimmermann, A. Filipovic, H.-F. Schleiermacher, J. Greulich, S. Rousu, J. Hast, R. Myllylä, U. Würfel, Aerosol jet printed grid for ITO-free inverted organic solar cells, Sol. Energy Mater. Sol. Cells 107 (2012) 252–258.

[22] R. Eckstein, G. Hernandez-Sosa, U. Lemmer, N. Mechau, Aerosol jet printed top grids for organic optoelectronic devices, Org. Electron. 15 (September (9)) (2014) 2135–2140.

[23] A. Mette, P.L. Richter, M. Hörteis, S.W. Glunz, Metal aerosol jet printing for solar cell metallization, Prog. Photovoltaics 15 (November (7)) (2007) 621–627.

[24] M. Hörteis, S.W. Glunz, Fine line printed silicon solar cells exceeding 20% efficiency, Prog. Photovoltaics 16 (November (7)) (2008) 555–560.

[25] C. Yang, E. Zhou, S. Miyanishi, K. Hashimoto, K. Tajima, Preparation of active layers in polymer solar cells by aerosol jet printing, ACS Appl. Mater. Interfaces 3 (September (10)) (2011) 4053–4058.

[26] L. Zhou, J.Y. Zhuang, M.S. Song, W.M. Su, Z. Cui, Enhanced performance for organic light-emitting diodes by embedding an aerosol jet printed conductive grid, J. Phys. D: Appl. Phys. 47 (March (11)) (2014) 115504.

[27] K.K. Christenson, J.A. Paulsen, M.J. Renn, K. McDonald, J. Bourassa, Direct printing of circuit boards using aerosol Jet®, in: International Conference; 27th, Digital Printing Technologies; Digital Fabrication; 2011, Minneapolis, MN, 2011.

[28] R.C. Roberts, N.C. Tien, Multilayer passive RF microfabrication using jet-printed au nanoparticle ink and aerosol-deposited dielectric, Solid-State Sensors, Actuators and Microsystems (Transducers & Eurosensors XXVII), 2013 Transducers & Eurosensors XXVII: the 17th International Conference on, Barcelona (2013).

[29] P. Choi, N.H. Jalani, R. Datta, Thermodynamics and proton transport in nafion II. Proton diffusion mechanisms and conductivity, J. Electrochem. Soc. 152 (February (3)) (2005) 123–130.

[30] S.J. Paddison, R. Paul, The nature of proton transport in fully hydrated Nafion, Phys. Chem. Chem. Phys. 4 (February (7)) (2002) 1158–1163.

[31] K. Sagarik, M. Phonyiem, C. Lao-ngam, S. Chaiwongwattana, Mechanisms of proton transfer in Nafions: elementary reactions at the sulfonic acid groups, Phys. Chem. Chem. Phys. 10 (February (15)) (2008) 2098–2112.

[32] Microchip Technology Inc, Microchip MCP3001 Datasheet, Microchip Technology Inc., 2007.

[33] P. Vanýsek, in: W.M. Haynes (Ed.), CRC Handbook of Chemistry and Physics, 93rd Edition, 93rd ed., CRC Press, Boca Raton, 2012, pp. 5–83.

[34] Lascar Electronics Easylog-data-logger EL-USB-2-LCD+, Lascar Electronics, [Online], 2017, Available: https://www.lascarelectronics.com/easylog-data-logger-el-usb-2-lcdplus/. (Accessed 22 February 2017).

[35] C.-D. Feng, S.-L. Sun, H. Wang, C.U. Segre, J.R. Stetter, Humidity sensing properties of Nation and sol-gel derived SiO2/Nafion composite thin films, Sens. Actuators B 40 (May (2–3)) (1997) 217–222.

[36] C. Sapsanis, U. Buttner, H. Omran, Y. Belmabkhout, O. Shekhah, M. Eddaoudi, K.N. Salama, A nafion coated capacitive humidity sensor on a flexible PET substrate, Circuits and Systems (MWSCAS), 2016 IEEE 59th International Midwest Symposium on, Abu Dhabi (2016).

[37] L.J. Deiner, T.L. Reitz, Inkjet and aerosol jet printing of electrochemical devices for energy conversion and storage, Adv. Eng. Mater. 19 (July (7)) (2017) 1600878, http://dx.doi.org/10.1002/adem.201600878.

[38] D. Pech, M. Brunet, P.-L. Taberna, P. Simon, N. Fabre, F. Mesnilgrente, V. Conédéra, H. Durou, Elaboration of a microstructured inkjet-printed carbon electrochemical capacitor, J. Power Sources 195 (4) (2010) 1266–1269.

[39] M. Cherrington, T.C. Claypole, D. Deganello, I. Mabbett, T. Watson, D. Worsley, Ultrafast near-infrared sintering of a slot-die coated nano-silver conducting ink, J. Mater. Chem. (21) (2011) 7562–7564.

[40] J. Perelaer, U.S. Schubert, Novel approaches for low temperature sintering of inkjet-printed inorganic nanoparticles for roll-to-roll (R2R) applications, J. Mater. Res. 28 (February (4)) (2013) 564–565, 73.

Biographies

Ben Clifford is a research assistant at the Welsh Centre for Printing and Coating in the College of Engineering, Swansea University. He recently submitted his Ph.D thesis in Aerosol Jet Deposition for the Development of Printed Electronics (Swansea University, 2016). His research is primarily focused on applications of aerosol jet deposition but also includes direct-write fabrication technologies, materials development and process optimisation.

Dr. David Beynon is a Research Officer active in the field of printed functional and active materials. Working in Swansea Universities College of Engineering he has expertise encompassing multiple printing processes and the application of those processes for the realisation of devices such as printed sensors.

Dr. Christopher Phillips is a lecturer in the College of Engineering, Swansea University. His research interests include functional ink formulation and printing for electronic, energy storage and biomedical applications.

Dr. Davide Deganello is an Associate Professor in the College of Engineering, Swansea University. He has a Ph.D. in Mechanical Engineering (Swansea University, 2008). His research interests comprise functional printing and additive processing for energy storage, electronic and biomedical applications, combined with study of underlying complex fluids rheology.